



UNIVERSITÀ POLITECNICA DELLE MARCHE  
Repository ISTITUZIONALE

## Experimental study on a Savonius wind rotor for street lighting systems

This is the peer reviewed version of the following article:

*Original*

Experimental study on a Savonius wind rotor for street lighting systems / Ricci, Renato; Romagnoli, Roberto; Montelpare, Sergio; Vitali, Daniele. - In: APPLIED ENERGY. - ISSN 0306-2619. - ELETTRONICO. - 161:(2015), pp. 143-152. [10.1016/j.apenergy.2015.10.012]

*Availability:*

This version is available at: 11566/228151 since: 2022-05-25T18:19:37Z

*Publisher:*

*Published*

DOI:10.1016/j.apenergy.2015.10.012

*Terms of use:*

The terms and conditions for the reuse of this version of the manuscript are specified in the publishing policy. The use of copyrighted works requires the consent of the rights' holder (author or publisher). Works made available under a Creative Commons license or a Publisher's custom-made license can be used according to the terms and conditions contained therein. See editor's website for further information and terms and conditions.

This item was downloaded from IRIS Università Politecnica delle Marche (<https://iris.univpm.it>). When citing, please refer to the published version.

(Article begins on next page)

# **Experimental study on a Savonius wind rotor for street lighting systems**

R. Ricci , R Romagnoli , S. Montelpare , D. Vitali

This is an accepted manuscript of the following article, published on publication in Applied Energy: S. Montelpare, R. Ricci , R Romagnoli , S. Montelpare , D. Vitali (2016) Experimental study on a Savonius wind rotor for street lighting systems. Applied Energy, Volume 161, 1 January 2016, Pages 143-152, <https://doi.org/10.1016/j.apenergy.2015.10.012>. It is deposited under the terms of Creative Commons Attribution-NonCommercial-NoDerivatives License, which permits non-commercial re-use, distribution and reproduction in any medium. The provided original work is properly cited, and it is not altered, transformed or built upon in any way.

Original work available at:

<https://doi.org/10.1016/j.apenergy.2015.10.012>

# Experimental study on a Savonius wind rotor for street lighting systems<sup>☆</sup>

Renato Ricci<sup>a</sup>, Roberto Romagnoli<sup>a,\*</sup>, Sergio Montelpare<sup>b</sup>, Daniele Vitali<sup>a</sup>

<sup>a</sup>*Department of Industrial Engineering and Mathematical Sciences (DIISM)  
Polytechnic University of Marche, via Breccie Bianche 1, 60131 Ancona (Italy)*

<sup>b</sup>*Department of Engineering and Geology (INGEO), University of Chieti-Pescara, viale Pindaro 42, Pescara (Italy)*

---

## Abstract

This paper investigates the aerodynamic performance of a Savonius vertical axis wind rotor to be used in an innovative lamp post. The wind generator is the main part of a public lighting system (a street lamp) powered by both Aeolian and Solar renewable energy sources. This study is aimed to analyze the effects of different constructive solutions on the rotor performance. Experimental dynamic tests were performed on a 1:1 rotor model in the Environmental Wind Tunnel (EWT) of Polytechnic University of Marche (UNIVPM); tests were performed at different wind velocities and for several combinations. Obtained results confirmed that, in the tested range  $2 - 3.3 \times 10^5$ , the rotor performance do not depend on Reynolds number. Tests also show that end plates and blades overlap increase the  $C_{P,max}$ , while external grids and structural posts have negative effects on the rotor performance. Best results were obtained for a configuration having an helical rotor with a  $105^\circ/m$  twist, open blades overlap and end plates.

**Keywords:** wind tunnel, experimental measurements, Savonius rotor, wind energy, street lamp, renewable energies

---

## 1. Introduction

Last decades were characterized by a growing interest on environmental issues and consequently on energy topics. Several researchers have dedicated their attention to study alternative energy production sources; i.e. the use of renewable energies and smart energy production systems can effectively contribute to reduce environmental impacts. Following this line, a smart lamppost, powered by renewable energy sources, was developed at University "Politecnica delle Marche" (UNIVPM): the basic idea was to develop a system to be used in urban environments in network or standalone configurations. The proposed street light is powered by both solar and wind energies: the former is supplied by a photovoltaic panel placed on the upper end of the lamppost, the latter by three vertical axis wind rotors (VAWT) inserted, in line,

---

<sup>☆</sup>This document is a collaborative effort.

\*Corresponding Author

Email addresses: [ricci@univpm.it](mailto:ricci@univpm.it) (Renato Ricci), [r.romagnoli@univpm.it](mailto:r.romagnoli@univpm.it); [roberto.r73@gmail.com](mailto:roberto.r73@gmail.com) (Roberto Romagnoli), [s.montelpare@unich.it](mailto:s.montelpare@unich.it) (Sergio Montelpare), [d.vitali@univpm.it](mailto:d.vitali@univpm.it) (Daniele Vitali)

---

## Nomenclature

$A$	rotor swept area [ $m^2$ ]	$s$	buckets spacing distance [ $m$ ]
$A_t$	total frontal area (rotor + frame) [ $m^2$ ]	$S$	test section area [ $m^2$ ]
$a$	buckets overlap distance [ $m$ ]	$T$	torque [ $Nm$ ]
$c$	bucket chord [ $m$ ]	$v_\infty$	free stream velocity [ $ms^{-1}$ ]
$C_P$	power coefficient	$v$	contract section velocity [ $m/s$ ]
$C_T$	torque coefficient	<i>Greek</i>	
$C_{TS}$	static torque coefficient	$\epsilon$	blockage factor
$D$	rotor diameter ( $D = 2R$ ) [ $m$ ]	$\lambda$	tip speed ratio
$D_{ep}$	end plates diameter [ $m$ ]	$\lambda_c$	tip speed ratio at which $C_{P,max}$ occurs
$d$	shaft diameter [ $m$ ]	$\nu$	air cinematic viscosity
$H$	turbine height [ $m$ ]	$\sigma$	standard deviation
$l$	lever arm length [ $m$ ]	$\omega$	angular velocity [ $rad/s$ ]
$P$	power [ $W$ ]	$\theta$	position angle [ $^\circ$ ]
$R$	rotor radius [ $m$ ]	<i>Subscripts</i>	
$Re$	Reynolds number	$max$	maximum value

---

along the support structure (Figure 1). The concept to use different energy sources was derived from the aim to design a standalone system able to have several days of self-sufficiency; i.e. a windy day normally corresponds to a cloudy sky, with low photovoltaic production, and inversely a sunny day corresponds to low wind velocities, with small aeolian production. By combining both energy sources it could be possible to extend the potentiality of a standalone system [1].

The choice to use a Savonius wind rotor derives from several positive considerations: it is very simple to realize, economic, compact and has low noise emissions. Besides it works with turbulent and fluctuating wind conditions typical of urban environments, has an high static torque (self starting wind turbine), requires little maintenance and could be easily integrated into design of vertical structures. On the other side the Savonius power performance are lower than three blades horizontal axis wind turbines and so it should be not intended for significant energy production. Many authors have studied the Savonius wind rotor, obtaining maximum power coefficients in the range 0.10 - 0.25. As just mentioned, these are low values if compared to those obtained with other types of wind generators [2, 3]; this reason has led to a large number of numerical and experimental works analysing the factors that could improve the rotor performance. This paper deals again with these topics because of not all variables have been fully investigated and several divergences can be found in literature. Moreover the investigated Savonius rotor was designed to be implemented inside a



Figure 1: The UNIVPM prototype of the experimental street lamp powered by renewable sources.

street lamp and, due to practical constructive choices, different geometric parameters had to be used, some of which not present in literature. For these reasons they were necessary experimental tests in order to evaluate the influence of geometric and constructive parameters on the rotor performance. Experimental measurements were performed in the Environmental Wind Tunnel (EWT) of the UNIVPM. Tests were executed in dynamic conditions on a 1:1 scale model; the rotor twist, the presence of end plates, the effects of blades overlap and the presence of support posts were analysed. Results are illustrated in terms of  $C_P - \lambda$  and  $C_T - \lambda$  plots for all the different combinations of the tested elements.

## 2. The Savonius rotor

The selected wind rotor is named Savonius with reference to the Finnish engineer S.J. Savonius, owner of its first patent, which dates back to 1930s [4, 5]. It is a vertical axis wind rotor having a simple geometry. In its most common shape it is made of two semi-cylindrical blades, asymmetrically positioned with respect to the vertical axis of rotation. Motion is generated by unbalanced aerodynamic forces acting on the advancing bucket, which is hit by the flow on its concave side, and the returning bucket, which moves in the opposite direction of the air flow. The concurrent forces system produces a resultant moment along the rotational axis of the rotor, which makes the system rotate. Due to its simple geometry, the Savonius rotor was also used as water turbine with an horizontal axis configuration [6, 7]. According to literature, its geometry can be described by few parameters that are illustrated in Figure 2. Savonius turbine is classified as a drag devices because of the main forces acting on the blades are related to the aerodynamic pressure drag, but a well designed rotor can reach tip speed ratios  $\lambda$  higher than 1.0 (eq. (3)); this result indicates rotational speeds higher than the inlet wind velocity and this is possible only for a rotor also having a lift behaviour.

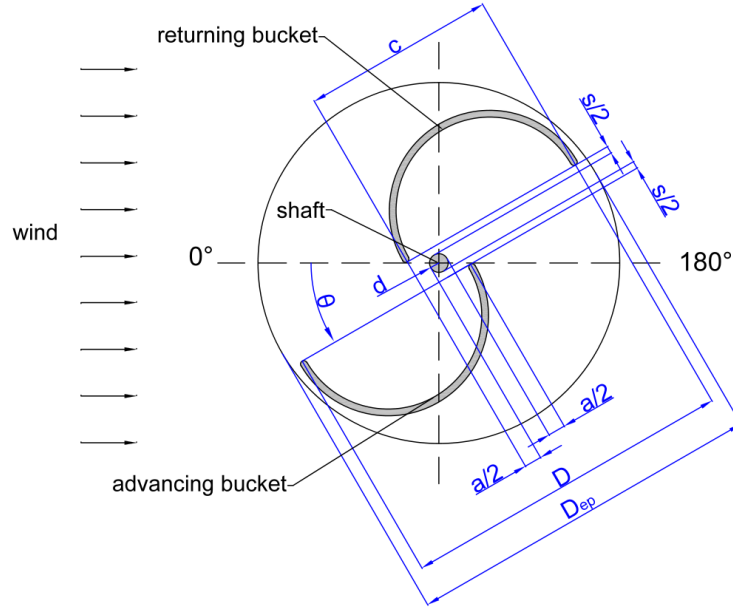


Figure 2: Schematic representation of a classic Savonius rotor section.

First investigations, available in literature, have been experimental studies with flow visualizations [8–11], or experimental tests aimed to measure the average performance of the rotor in terms of static torque and power coefficient [12]. At a later stage many studies tried to analyse the rotor by measurements of the surface pressure distribution over a single blade (e.g. [13–18]). In the same period was introduced a first numerical approach using the discrete vortex method to evaluate the flow field of a Savonius rotor [19–21]. In recent years several authors have used new techniques, as P.I.V. [22] or C.F.D. (e.g. [23–27]), in order to analyse the fluid dynamic flow field, while others have focused their attention on techniques able to maximize the rotor performance [6, 28–32].

Despite this large number of studies, many authors have reached contrasting conclusions on the role of the geometrical parameters of the rotor.

As example several authors have been positively evaluated the presence of an "open overlap" [12, 17, 18, 21, 33], and have agreed in suggesting an optimum overlap ratio between 10 and 15%. In these conditions it is possible to observe a jet flow trough the overlap that increases the pressure on the concave side of the returning blade, thus reducing the overall drag [23]. Conversely other authors negatively evaluate the presence of open overlap if applied to slightly modified geometries [14, 34].

A general agreement can be observed in literature about the periodic behaviour of the torque angular distribution, with a periodicity equal to the number of rotor blades [34, 35]. Measurements of the static torque at different rotor angular positions have revealed significant variations; it is possible to observe both high positive values, that are useful to start the rotor, and negative values, that can give starting problems

at certain wind angles. Besides these oscillations may cause unpleasant cyclic stresses to the structure [36]. Such problems can be overcome by employing rotors with an higher number of blades, with staggered stages [36–39], or alternatively by using blades twisted along their vertical axis. Also in this case there are however different opinions in literature: as example [40, 41] have observed that the twist or the addition of stages increase the maximum  $C_P$  of the rotor, while others like [35] has measured an opposite result.

Likewise the analyses about fluid dynamic parameters have often led to conflicting results: some authors affirm that the Reynolds number affects both the power coefficient [39, 42] and the static torque coefficient ( $C_{TS}$ ) [35], others only  $C_{TS}$  [12], still others affirm that it has no influence over the rotor performance because of they relate differences to the friction of the bearings used in the experimental set-up [14].

Further informations about results of experimental analyses performed on these and many other parameters can be found in [43], where author offers an extensive and accurate review of the experimental literature on Savonius rotors.

The wind turbine investigated in this work is the "classic" Savonius rotor with circular blades; its geometric characteristics are illustrated in 3.2. Many authors (e.g. [12, 18, 36, 44]) have suggested, for this kind of rotor, an optimal configuration which characteristics are shown in Table 1. Several of these parameters have been adopted for the Savonius rotor tested in this paper, but some were modified (Table 2) in order to: facilitate the industrial production (as example the choice to use multiple rotor stages rather than twisted blades), improve the structural stiffness (as example modifying the central shaft diameter and the overlap ratio) and favour integration inside the lamppost (as example increasing the aspect ratio).

Optimal solution			
number of buckets	2	helical step	0°/m
overlap ratio (a/c)	10-15 %	shaft presence	no
spacing ratio (s/c)	0	number of stages	2
aspect ratio (H/D)	1-1.2	angle between stages	90°
bucket arc angle	180°	$C_{P,max}$ (1 stage)	$\simeq 0.24$
end plates $D_{ep}/D$	1.1	$C_{P,max}$ (2 stages)	$\simeq 0.28$

Table 1: Optimal configuration for a Savonius rotor with semi-circular blades.

### 3. Experimental apparatus

#### 3.1. The Environmental Wind Tunnel (EWT)

The EWT is a closed circuit wind tunnel as shown in Figure 3. The test section has a cross square area of  $3.16 \text{ m}^2$  and is subdivided in three main subsections: the former is used for aerodynamic tests that require a uniform velocity distribution and low turbulence levels. The second one is used to measure the effects of reciprocal interferences between slender bodies. The latter is the environmental section and is used

to test wind effects over buildings, structures and orography models that are immersed into fully developed environmental boundary layers. Wind tunnel is equipped with a fan having a constant rotational speed of

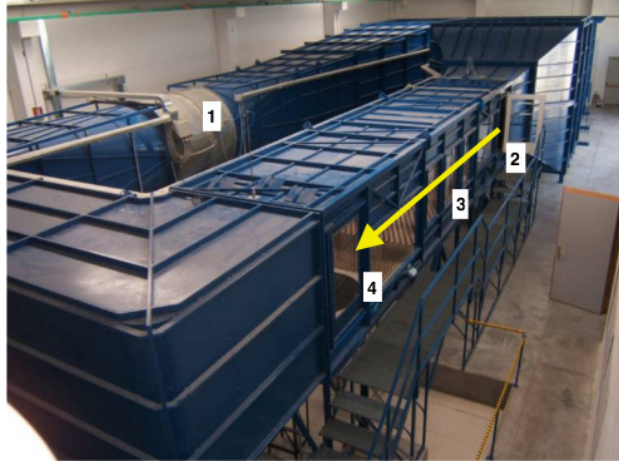


Figure 3: The Environmental Wind Tunnel of the University "Politecnica delle Marche": 1-fan 2-first test subsection 3-second test subsection 4-third test subsection.

975 RPM and 16 blades with an adjustable pitch. The average wind speed inside the test section ranges between  $6 \text{ m/s}$  and  $40 \text{ m/s}$ . Measurements carried out with a Constant Temperature Hot Wire Anemometer (CTA HWA) have shown a 2-D inlet speed uniformity within 2.5% and a turbulence intensity lower than 0.3%. Wind tunnel is also equipped with a compact heat exchanger, that is used to limit temperature fluctuations within a range of  $1 \text{ }^{\circ}\text{C}$ .

### 3.2. The rotor models

Rotors presented in this research work are Savonius type with semi-circular blades; they are realized in a 1:1 scale with respect to those designed for the street lamp. The models have a diameter  $D$  of  $0.384 \text{ m}$  and are  $1 \text{ m}$  high. The section swept by the rotor is therefore of  $0.384 \text{ m}^2$ , while the blockage factor, introduced by [45] and defined in eq. (1), is 3.2 %. Considering also the experimental set-up support structure (fixed frame), the total blockage area reaches a maximum of 6.1 %. According to eq. (2), introduced in [45], a correction coefficient was applied to the inlet velocity so to take into account the blockage effect:

$$\epsilon = \frac{A_t}{4S} \quad (1)$$

$$v = v_{\infty}(1 + \epsilon) \quad (2)$$

The rotor is an assembly of modular elements axially connected along a central shaft, having a diameter  $d$  of  $37 \text{ mm}$ , so to form a "skeleton". Such elements can be aligned or staggered by regular angles with respect to the vertical axis. In this way it is possible to realize a rotor having a straight or a twisted geometry (i.e.



an helical rotor). In this work three rotors have been analysed (Figure 4): two helical rotors with overall twists respectively of  $90^\circ$  and  $105^\circ$  and a straight rotor ( $0^\circ$ ). The  $105^\circ$  twist was a technical specification limit fixed by industrial partners appointed to realize the final prototype. The rotor blades surfaces were realized with a polyethylene sheet stretched upon the assembled skeleton; this polymeric material allowed to follow the double curvature given by the twist. The sheet is fixed to the modular ribs and stretched so as to have a solid and regular surface for the flow. The rotor central shaft and the blades tips are not in contact and rather they form a gap of  $18\text{ mm}$  where the flow can pass through.

Referring to Figure 2, the geometric characteristics of the tested rotors are summarized in Table 2.

Adopted solution			
number of buckets	2	helical step	$0\text{-}90\text{-}105^\circ/\text{m}$
overlap ratio (a/c)	8.2 %	shaft diameter ( $d$ )	37 [mm]
spacing ratio (s/c)	0	number of stages	1
aspect ratio (H/D)	2.6	bucket arc angle	$180^\circ$
end plates $D_{ep}/D$	no / 1.1	rotor diameter ( $D$ )	384 [mm]

Table 2: Geometric parameters of the rotors tested.

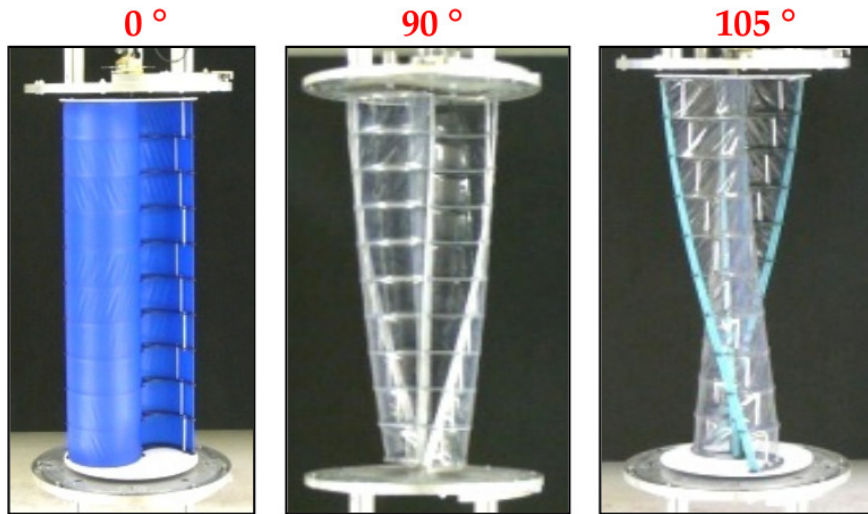


Figure 4: The rotors tested in the present work

By comparing these parameters with those in Table 1, it is possible to observe that the design choices have required a geometry different from the optimal one. Also for this reason it was necessary to perform an experimental analysis that accurately determines the role of the varied construction parameters: i.e. end plates, helical step and central gap. Another parameter that was tested is the presence of lamppost support poles placed externally to the rotor; indeed the street lamp concept provides four steel tubular posts

designed to the structural resistance. In this way the helical rotors do not have to support the weight of the structure and therefore lighter materials can be used.

#### 4. The measurements setup and procedure

In order to obtain  $C_P$  and  $C_T$  vs.  $\lambda$  curves for all the tested configurations, both wind speed and rotor angular velocity should be varied. The wind speed can be changed by adjusting the wind tunnel inlet flow velocity. The rotor angular velocity is varied by an hydraulic brake that clamps a disk coupled to the rotor shaft (Figure 5) and changes the counteracting torque; in the real case this action is performed by the torque of the electric generator coupled to the Savonius rotor. The testing procedure provides the subsequent steps: first of all a desired wind speed is selected, then the hydraulic brake is modulated on all its braking range, from null to full. In this way the system stabilises at different equilibrium states between the driving forces (fluid dynamics actions) and the resistant torque (braking friction loads) and it is possible to obtain enough operational points to draw the rotor characteristic curves.

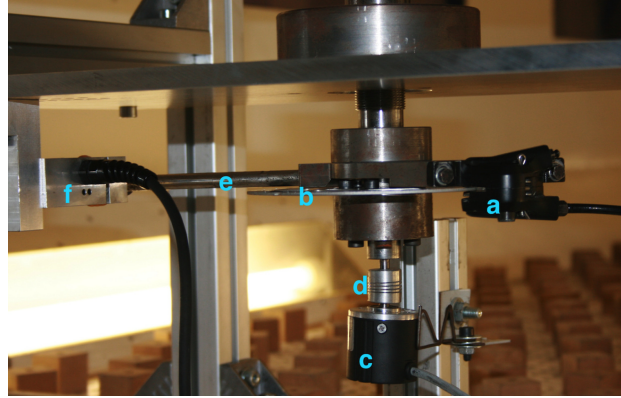


Figure 5: Details of the experimental apparatus: a) brake caliper b) break disk c) encoder d) joint e) lever arm f) load cell

Torque and power coefficients  $C_T$  and  $C_P$ , as also the  $\lambda$  tip speed ratio, are obtained, according to eq. (3)-(4), by measuring at the same time the torque  $T$  and the angular velocity  $\omega$ .

$$C_T = \frac{T}{0.5 \rho A R v^2} \quad \lambda = \frac{2\pi R \omega}{60 v} \quad (3)$$

$$C_P = \frac{P}{0.5 \rho A v^3} = \lambda C_T \quad (4)$$

The measurement apparatus is illustrated in Figure 5. The angular velocity  $\omega$  is directly acquired as RPMs by an incremental encoder. A radial lever arm, integrated within the braking system, transmits the torque  $T$  to a mono-axial load cell fixed to the set-up frame. The load cell was calibrated before the tests, using

sample weights. The torque is obtained from the simple relationship  $T = F l$ , where  $F$  is the force measured on the load cell and  $l$  the length of the lever arm.

Tests were performed at different inlet flow velocities; a National Instrument data acquisition system was used for a real-time analysis of the experiment. Data were collected with an acquisition period of 3 seconds and with a sampling rate of 1024 Hz.

## 5. Evaluation of measurement uncertainties

Measured quantities are affected by several sources of uncertainty, that are normally classified as type A or type B. Type A uncertainties arise from factors that cannot be kept under control or whose effect cannot be reasonably determined “a priori”. They are usually associated with random fluctuations that occur during acquisitions. Given a population standard deviation  $\sigma$  of the  $N$  values read in single acquisition, the mean value that can be extracted is subjected to an uncertainty given by eq. (5).

$$\sigma_{ave} = \frac{\sigma}{\sqrt{N}} \quad (5)$$

Type B uncertainties are those already known or that can be evaluated “a priori” on the basis of the possible sources of error. In our case they are related to calibration and accuracy of the sensors. Type A uncertainties were evaluated with the least squares straight line method, while type B uncertainties were directly derived from the technical specifications of the instruments. When this latter information was not available, a rectangular error distribution was assumed, which can match the standard deviation of a normal distribution by dividing the maximum error of the instrument by a factor  $\sqrt{3}$ . If none of the two types of error includes the other, the uncertainty of the quantities directly measured is obtained according to eq. (6). For the derived quantities, the error propagation law was used (7).

$$\sigma = \sqrt{\sigma_A^2 + \sigma_B^2} \quad (6)$$

$$f = f(x, y) \implies \sigma_f = \sqrt{\left(\frac{\partial f}{\partial x} \sigma_x\right)^2 + \left(\frac{\partial f}{\partial y} \sigma_y\right)^2} \quad (7)$$

A 95% confidence level, corresponding to an interval of  $\pm 2\sigma$ , was chosen in order to evaluate extended uncertainties. Experimental tests have shown a  $\sigma$  mean value of 2,37% for uncertainties associated with the single acquisitions, while the error associated with the  $\sigma_{ave}$  average acquisition value is approximately 0,07%.

## 6. Experimental Results

Several combinations of the parameters to be investigated were tested in the experimental analyses. These configurations are summarized in Table 3, where the corresponding reference codes are listed. Each

Test code	Helical step (°/m)	End Plates (E)	Posts (P)
0deg_nE_nP	0	no	no
0deg_yE_nP	0	yes	no
0deg_nE_yP	0	no	yes (4)
0deg_yE_yP	0	yes	yes (4)
90deg_nE_nP	90	no	no
90deg_yE_nP	90	yes	no
90deg_nE_yP	90	no	yes (4)
90deg_yE_yP	90	yes	yes (4)
90deg_yE_yP3	90	yes	yes (3)
105deg_nE_nP	105	no	no
105deg_yE_nP	105	yes	no
105deg_nE_yP	105	no	yes (4)
105deg_yE_yP	105	yes	yes (4)

Table 3: Legend of the main configurations tested.

of the listed configurations was tested in dynamic conditions at different wind velocities  $v$ . The  $T$ ,  $P$  vs  $\omega(rpm)$  curves as well as the curves of the  $C_T$  e  $C_P$  vs  $\lambda$  coefficients were extracted.

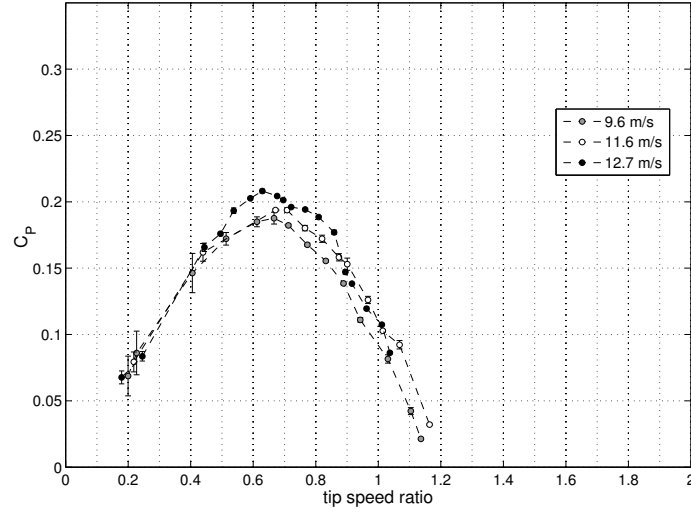
### 6.1. Effect of the Reynolds number

As previously mentioned, researchers do not agree on the role of the Reynolds number on the performance of Savonius turbines. Some claim a Reynolds number dependency, while other assert that the observed different values of torque and power coefficients, obtained at different  $Re$ , are related to the friction of the bearings. Although frictions were not directly measured, a comparison using two different experimental layouts was carried out in this work: the first layout (I) was equipped with small bearings (SKF 4205ATN9, internal diameter 25 mm, external diameter 52 mm, and SKF 6304, internal diameter 20 mm, external diameter 52 mm), the second layout (II) was assembled with considerably oversized bearings (SKF 5306, internal diameter 30 mm, external diameter 72 mm, and SKF 6008, internal diameter 40 mm, external diameter 68 mm). The comparison was made using a rotor with no twist, no end-plates, no posts and with an open overlap (0deg\_nE\_nP). Results are shown in Figure 6 and Figure 7, while velocities and Reynolds numbers are illustrated in Table 4.

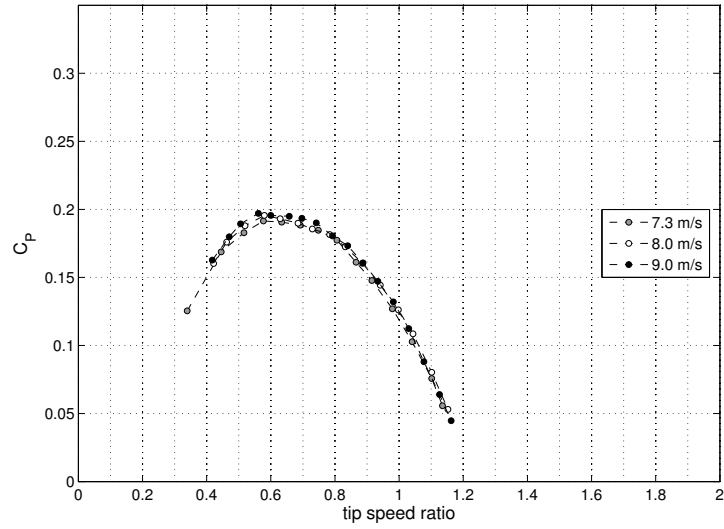
The Reynolds number was calculated according to eq. (8). The dynamic viscosity  $\nu$  was calculated using the air temperature measured with a properly calibrated RTD PT100.

$$Re = \frac{v D}{\nu} \quad (8)$$

Both tests show identical trends, although the curves carried out with the first assembly (test I) show a small reciprocal divergence at different velocities. Tests with the big bearings (II) was carried out at lower

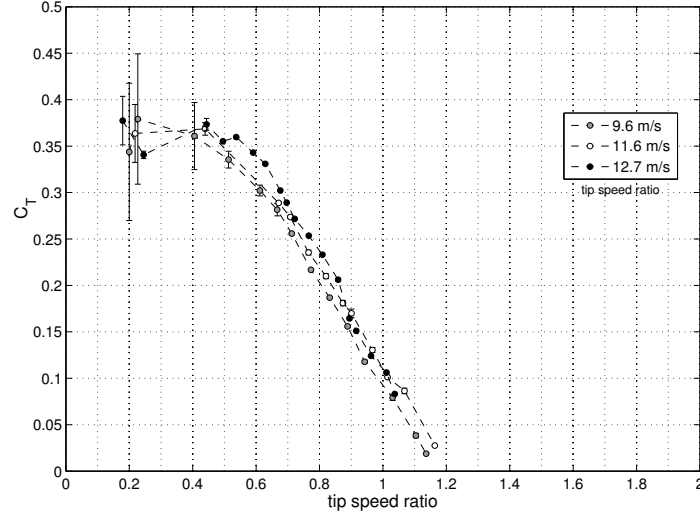


(a) set-up with the small bearings (test I)

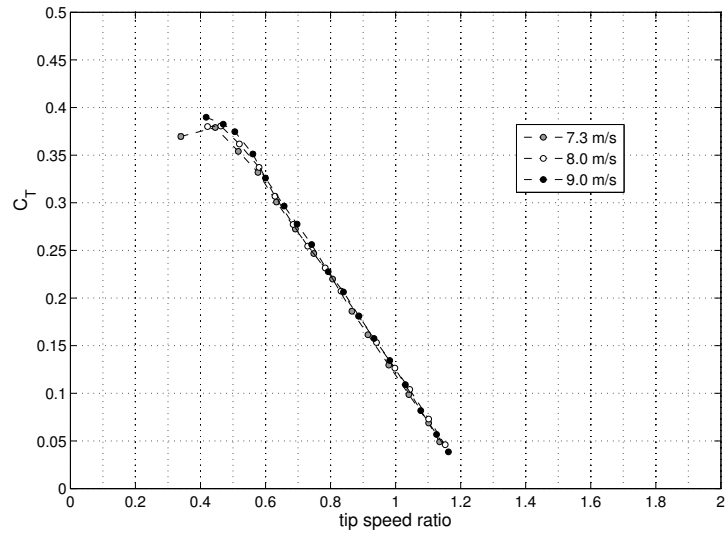


(b) set-up with the big bearings (test II)

Figure 6: Effect of the Re number on the  $C_P$  curves.



(a) set-up with the small bearings (test I)



(b) set-up with the big bearings (test II)

Figure 7: Effect of the  $Re$  number on the  $C_T$  curves.

air speed $v_\infty$	corrected speed $v$	Re number (I)	Re number (II)
6.9	7.3	—	199'940
7.7	8.1	—	221'851
8.5	9	—	246'501
9.1	9.6	249'629	—
11	11.6	301'635	—
12	12.7	330'238	—

Table 4: Velocities and Re numbers for the tests of Figure 6 and 7.

velocities to enhance the relative weight of bearing friction, but the curves perfectly overlap. This indicates that  $C_P$  and  $C_T$  are independent of the inlet flow selected velocities and, therefore, of the Reynolds number. It is besides plausible to affirm that discrepancies observed in tests with small bearings are due to the greater effects of the mechanical frictions. By regressing the experimental data with a least squares third order polynomial curve is possible to obtain a  $C_{P,max} = 0.189$  at  $\lambda = 0.67$  for test (I), and a  $C_{P,max} = 0.192$  at  $\lambda = 0.65$  for test (II); i.e. negligible differences.

## 6.2. Effect of the end plates

End plates are built in form of circular discs applied to both the ends of the rotor. Their effect is illustrated in Figure 8 for the straight rotor and in Figure 9(a) and 9(b) for the helical ones.

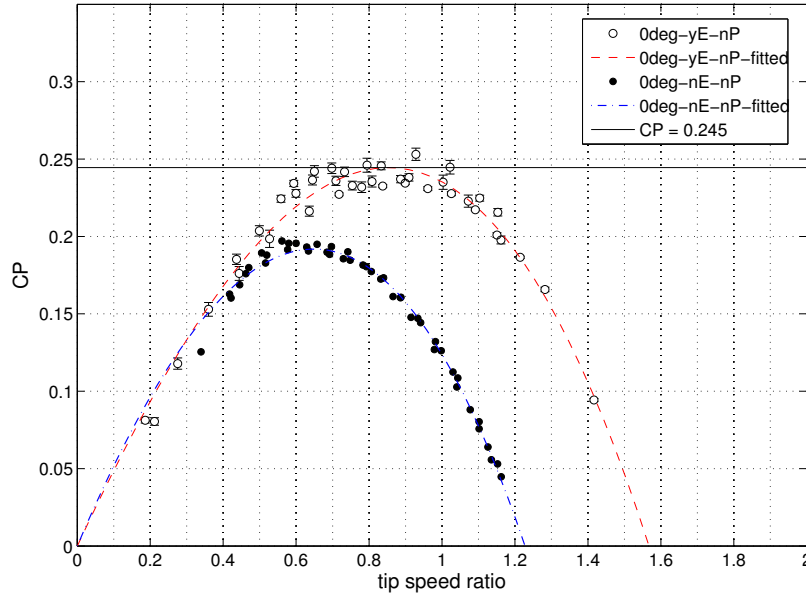
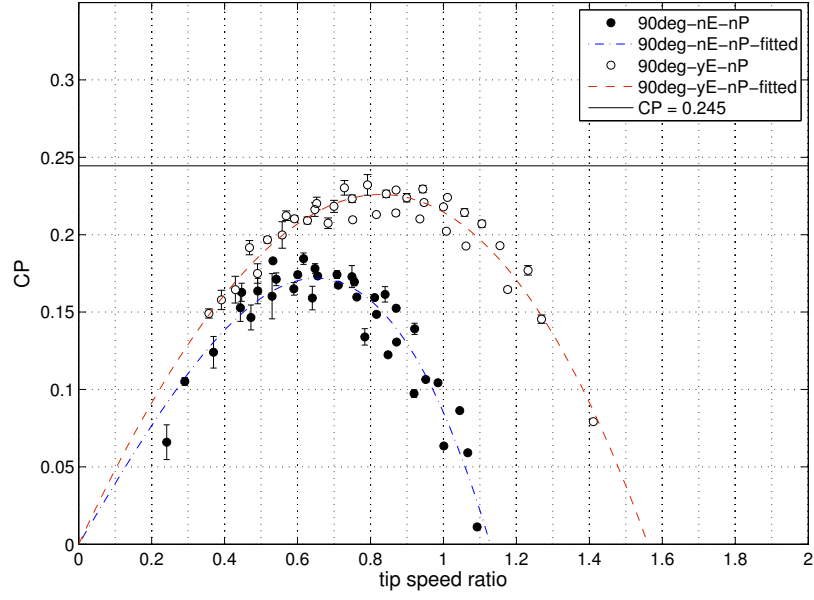
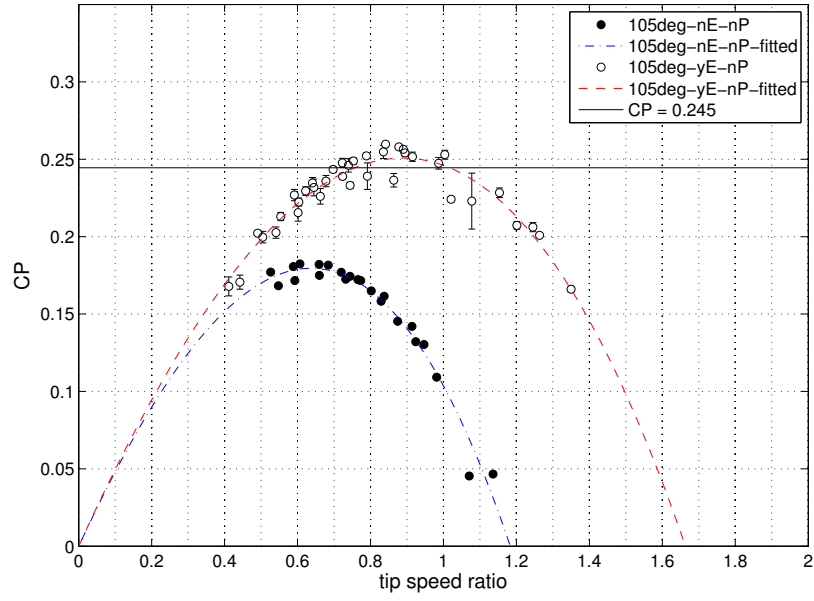


Figure 8: End Plates effect (rotor with no helical step).



(a) Rotor with  $90^\circ/\text{m}$  helical step.



(b) Rotor with  $105^\circ/\text{m}$  helical step.

Figure 9: End plates effect on helical rotor efficiency  $C_P$ .



Graph points refer to the experimental values obtained at different wind velocities, while the fitting curve was obtained from a least squares third order polynomial regression on all acquired data. An improvement effect, due to the confinement of the flow inside the rotor, is observable and confirms literature results. In our case, the improvement of the peak of  $C_P$ , as calculated from the fitting curve, is between 27% and 39%; refer to Table 5. In order to simplify the comparison among the different configurations, an horizontal line, corresponding to the maximum  $C_P$  of a reference test, is shown in the graphs. This reference is the straight rotor with end-plates (0deg\_yE\_nP), which corresponds to the most frequent configuration observed in literature.

Helical step (°)	0	90	105
without End Plates	0.192	0.172	0.18
with End Plates	0.245	0.226	<b>0.251</b>
variation	+27 %	+31 %	<b>+39 %</b>

Table 5: The  $C_{P,max}$  with the presence of End Plates.

### 6.3. Effect of the helical step

The effect of the helical twist can again be deduced from Table 5, and in Figure 10 the results for the rotors with end plates are illustrated. It can be noticed that for a configuration with end plates, which resulted a greater choice, the rotor with a step of 90° has a slightly lower  $C_{P,max}$ , with respect to a twist of 105 °; in absence of end plates, the helical step induces lower performance due to the augmented flow escape.

### 6.4. Effect of the posts

The posts are built as vertical cylindrical poles with a diameter of 42 mm and provide a structural support to the street lamp. They are placed externally at a distance of 635 mm from the center of the rotor and are arranged at every 90°. Experimental tests were performed with the orientation reported in Figure 11 in order to evaluate their greatest disturbance effect. Tests were performed by using both three and four posts. When measuring the configuration with three posts, the one upstream the rotor was removed (the circle filled with the gray color in Figure 11). Results of these tests are illustrated in Table 6 and in Figure 12, 13(a) and 13(b); it is possible to observe, as expected, a significant decrease in performance with four posts and a less evident effect in the case with three posts. This can be explained in two ways:

- the post upstream the rotor causes disturbance to the incident flow (leeward wake, flow deviation and overpressure on the incoming blade);
- the other posts cause only overpressures on the blades approaching them.

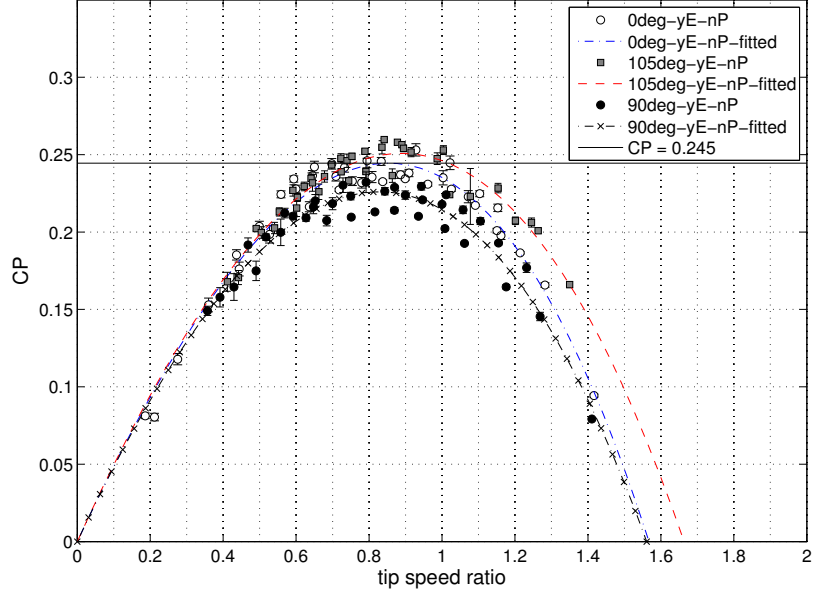


Figure 10: Effect of helical step on rotor efficiency  $C_P$  (rotors with End Plates).

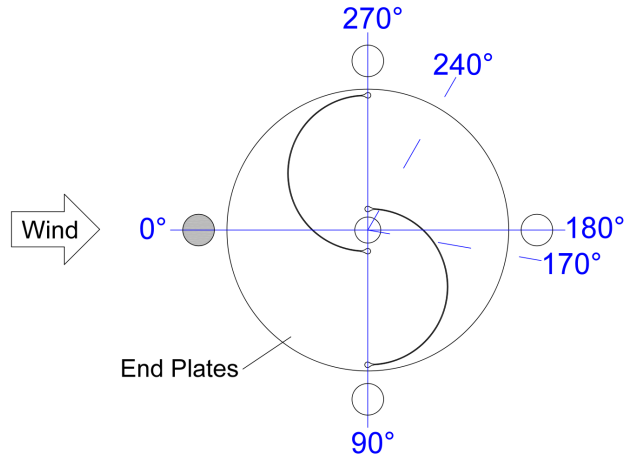


Figure 11: Posts position and used angular references. In tests with three posts the gray element is removed.

The last item allows to explain the lesser decrease of performance in test with three posts illustrated in Figure 12 and Figure 13(a). Finally it can be observed a difference in the effect of the posts depending on the twist: the rotor twisted by  $90^\circ$ , seems to suffer from this phenomenon more than the others. The better behaviour was experienced by the  $105^\circ$  due to the phase shift among the blade sections approaching to the post.

Posts	Helical step ( $^\circ/\text{m}$ )		
	0	90	105
no	0.245	0.226	<b>0.251</b>
3 posts	0.224 (-8.2 %)	0.195 (-13.7 %)	—
4 posts	0.187 (-23.4 %)	0.155 (-31.4 %)	0.206 (-17.9 %)

Table 6:  $C_{P,max}$  with the presence of posts.

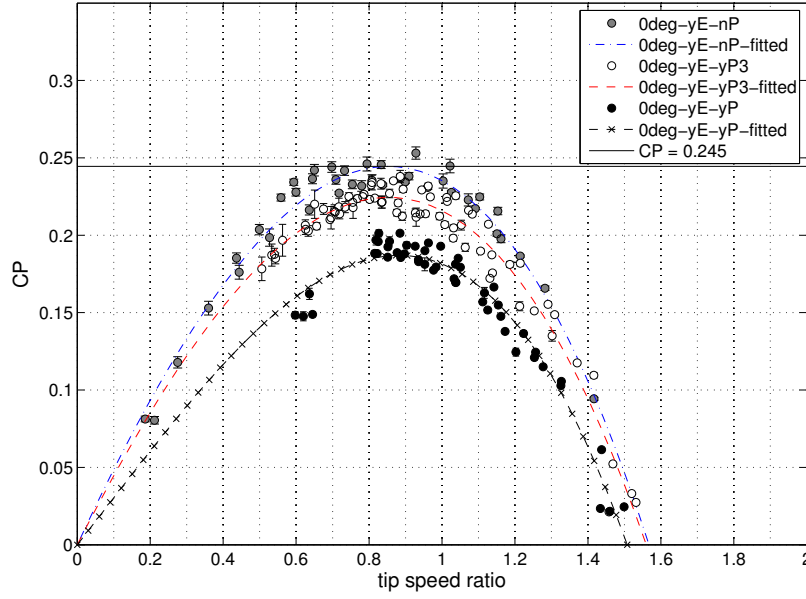
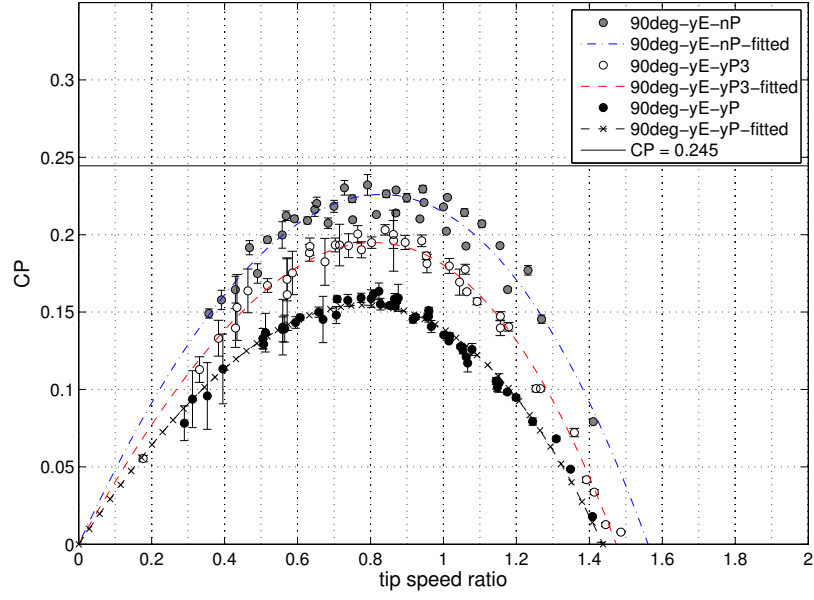


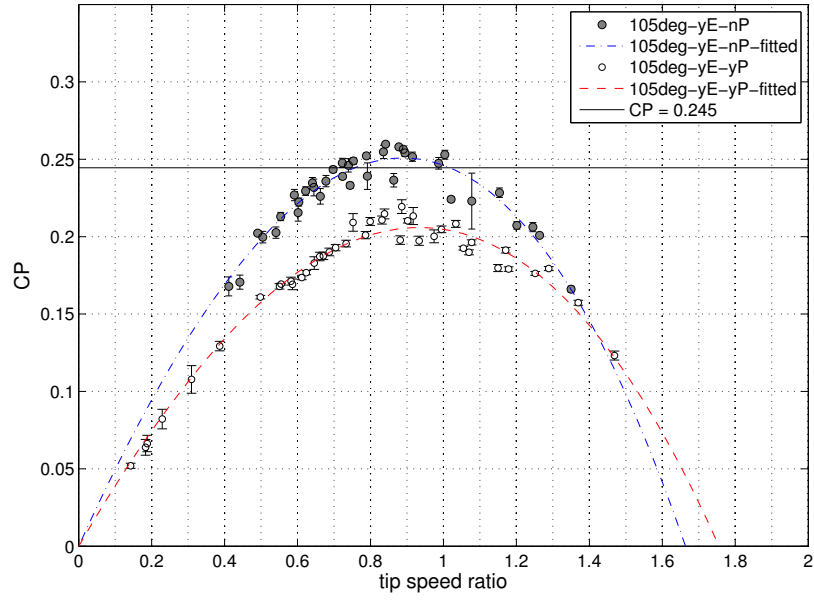
Figure 12: Effect of the posts on the rotor efficiency  $C_P$ .

### 6.5. External grid effect

An issue, that came out in the street lamp design process, was to test some systems to protect the rotating parts from collisions with external objects. A simple solution is a wire mesh to be placed externally to the wind rotors. These grids provide an adequate mechanical protection but they also induce pressure drops in the flow: this could negatively affect the performance of the wind rotor by reducing the available wind dynamic pressure to be converted. In order to evaluate such effects, different configurations were tested



(a) Rotor with 90°helical step.



(b) Rotor with 105°helical step.

Figure 13: Effect of the posts on the helical rotor efficiency  $C_P$ .

using two different wire meshes with square openings: the former has a square side length of 1 cm (normal grid), the latter has a side of 6 cm (wider and lighter grid). The ratio between the total area and the mesh open area, defined as porosity, is of the 70% in the first case and 95% in the second one. Tests were performed on the 105° helical rotor without end plates and results are shown in Figure 14. Experiments have showed that rotor performance strongly decrease (-32 % on  $C_{P,max}$ ) by placing a normal grid on the whole rotor circumference (black circles). So a gradual increase of the porosity was performed by lightening the normal grid in different positions (see Figure 14):

- in the frontal zone (LGa, white circles);
- in the frontal and in the back zone (LGab, white triangles);
- in the advancing bucket side (LGc, blue triangles);
- in the most part of the rotor (LGd, red square).

Finally a last configuration without any grid in the advancing bucket side (black square) was tested. Results show that all adopted solutions reduce rotor performance in a similar way but the worst solution is the configuration with the normal grid (black circles). The main numerical results are reported in Table 7.

Code	Light grid (LG)	Normal grid (G)	$C_{P,max}$
105deg_nE_nP	no	no	0.18
105deg_nE_yG	no	0°-360°	-32 %
105deg_nE_yG_LGa	0°-90°	elsewhere	-23 %
105deg_nE_yG_LGab	0°-90°, 170°-240°	elsewhere	-21 %
105deg_nE_yG_LGc	0°-180°	elsewhere	-18 %
105deg_nE_yG_LGd	0°-240°	elsewhere	-14 %
105deg_nE_yG180	no	180°-360°	-14 %

Table 7: Variation of the  $C_{P,max}$  with the presence of external grid (see also Figure 11).

## 6.6. Effect of the overlap

The influence of the overlap was examined by closing the gap near the rotational axis with an insulating tape. The helical rotor with a twist of 105° was used to analyse the jet-flow effect. Results illustrated in Figure 15 show that the absence of the gap causes a decrease of  $C_{P,max}$  by 17%.

## 7. Concluding remarks

This article reports the results of experimental tests performed in a wind tunnel on a Savonius wind rotor to be used on a street lamp powered by renewable energy. Practical design requirements and architectural restrictions impose some not optimal choices about the Savonius geometry as compared with scientific literature (as example an higher aspect ratio); this forces authors to carry out new experimental analyses

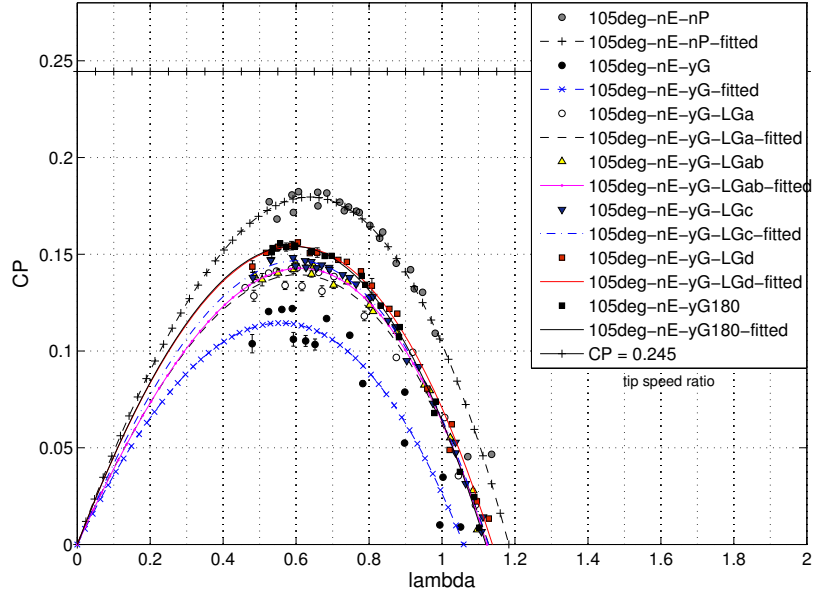


Figure 14: Grid effect (rotor with 105°h.s., no End Plates).

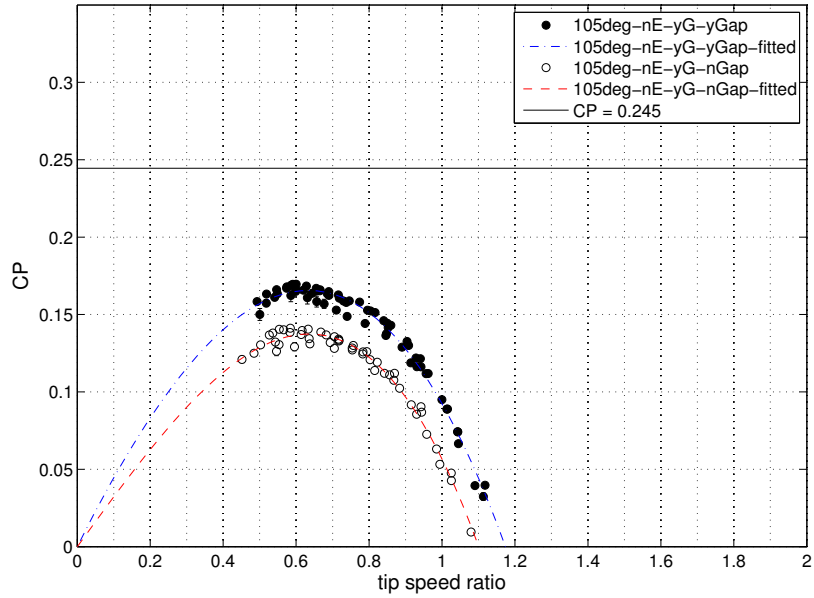


Figure 15: Open overlap effect (rotor with 105°h.s. and grid).

in order to redefine new optimal configurations and verify performance. Tests were carried out to evaluate the influence on the rotor performance of single or combined applications of: Reynolds number, helical step of 0, 90 and 105°, open overlap, end plates and external pillar posts. The overall results of the performed tests are shown in Table 8.

Test code	Helical Step (°/m)	End Plates (E)	Posts (P)	Light grid (LG)	Normal grid (G)	$C_{P,max}$	$\lambda_C$	$\lambda_{max}$
0deg_nE_nP	0	no	no	no	no	0.192	0.649	1.16
0deg_yE_nP	0	yes	no	no	no	0.245	0.854	1.57
0deg_yE_yP	0	yes	yes (4)	no	no	0.187	0.882	1.51
0deg_yE_yP3	0	yes	yes (3)	no	no	0.224	0.853	1.56
90deg_nE_nP	90	no	no	no	no	0.172	0.652	1.13
90deg_yE_nP	90	yes	no	no	no	0.226	0.828	1.56
90deg_yE_yP	90	yes	yes (4)	no	no	0.155	0.781	1.44
90deg_yE_yP3	90	yes	yes (3)	no	no	0.195	0.809	1.47
105deg_nE_nP	105	no	no	no	no	0.180	0.637	1.18
105deg_yE_nP	105	yes	no	no	no	<b>0.251</b>	0.889	1.66
105deg_yE_yP	105	yes	yes (4)	no	no	0.206	0.934	1.76
105deg_nE_yG	105	yes	yes	no	0-360°	0.122	0.597	1.07
105deg_nE_yG_LGa	105	yes	yes	0-90°	elsewhere	0.139	0.605	1.13
105deg_nE_yG_LGab	105	yes	yes	0-90+170-240°	elsewhere	0.143	0.612	1.13
105deg_nE_yG_LGc	105	yes	yes	0-180°	elsewhere	0.147	0.603	1.13
105deg_nE_yG_LGd	105	yes	yes	0-240°	elsewhere	0.154	0.597	1.14
105deg_nE_yG180	105	yes	yes	no	180-360°	0.154	0.590	1.12

Table 8: Summary of main experimental results.

The main findings of this study are instead hereinafter summarized:

- The tests were performed for Reynolds numbers between 200000 and 330000: in this range the performance ( $C_P$  e  $C_T$ ) were not dependent on the Reynolds number;
- The absence of the open overlap causes a decrease in the performance on  $C_{P,max}$  of about 17%;
- The helical rotor has lower performance than the straight rotor if the step is of 90°, (-6/7% on  $C_{P,max}$ ), while a twist of 105 ° shows similar performance;
- The end plates always have an improving effect, which however is greater for the helical rotor with a step of 105°, (+ 39% on  $C_{P,max}$ );
- The supporting posts negatively affect the performance due to two reasons:
  - a) leeward wake;
  - b) overpressure generated on the approaching blade;
- The negative effect of the posts, which can reach - 31.4% of  $C_{P,max}$ , is not the same for all rotors: the

effect is smaller for an helical rotor with a step of  $105^\circ$ , (-17.9%);

- External grids have a negative effect on the rotor performance depending on the grid position and porosity.
- Best results were obtained for an helical rotor with a step of  $105^\circ$ , with end plates and open gap; in this conditions a  $C_{P,max}$  of 0.251 at  $\lambda = 0.899$  was measured.

## 8. Acknowledgments

This work was realized thanks to the support of the projects IPA P.O.W.E.R.E.D and Ministry of Economic Development INDUSTRIA 2015 ([www.powered-ipa.it](http://www.powered-ipa.it)).

## 9. References

- [1] R. Ricci, S. Montelpare, D. Vitali, An innovative wind-solar hybrid street light: development and early testing of a prototype, *International Journal of Low-Carbon Technologies* 0 (2014) 1–10.
- [2] R. E. Wilson, P. B. Lissaman, *Applied Aerodynamics of wind power machines*, no. GI-41840 in *Research Applied to National Needs*, Oregon State University, 1974.
- [3] A. Jha, *Wind Turbine Technology*, ISBN 13: 978-1-4398-1507-6, CRC Press, 2011.
- [4] S. J. Savonius, The S-rotor and its applications, *Mechanical Engineering* 5 (53) (1931) 333–338.
- [5] S. J. Savonius, *The wing rotor in theory and practice*, Savonius Co., 1928.
- [6] K. Golecha, T. Eldho, S. Prabhu, Influence of the deflector plate on the performance of modified Savonius water turbine, *Applied Energy* (88) (2011) 3207–3217.
- [7] M. Khan, G. Bhuyan, M. Iqbal, J. Quaicoe, Hydrokinetic energy conversion systems and assessment of horizontal and vertical axis turbines for river and tidal applications: A technology status review, *Applied Energy* (86) (2009) 1823–1835.
- [8] G. von Bach, Untersuchungen fiber Savonius-rotoren und verwandte strömungsmaschinen, *Forsh. Geb. Ing.* 2 (1931) 218–231.
- [9] G. Bergeles, N. Athanassiadis, On the flow field around a Savonius rotor, *Wind Eng.* 6 (1982) 140–148.
- [10] G. J. Bowden, S. A. McAleese, The properties of isolated and coupled Savonius rotors, *Wind Eng.* 8 (1984) 271–288.
- [11] J. Massons, J. Gavalda, X. Ruiz, F. Diaz, Image analysis of the wake generated by a Savonius rotor, *Wind Eng.* 12 (1988) 341–351.
- [12] B. F. Blackwell, R. E. Sheldahl, L. V. Feltz, Wind tunnel performance data for two and three bucket Savonius rotors, United States Energy Research and Development Administration under contract AT .
- [13] A. Chauvin, D. Benghrib, Drag and lift coefficients evolution of a Savonius rotor, *Experiments in Fluids* 8 (1989) 118–120.
- [14] V. J. Modi, M. S. U. K. Fernando, On the performance of the Savonius wind turbine, *Journal of Solar Energy Engineering* 111 (1989) 71–81.
- [15] V. J. Modi, M. S. U. K. Fernando, N. J. Roth, *Aerodynamics of the savonius rotor: experiments and analysis*, vol. 5, IECEC, Energy Conversion Engineering Conference. Proceedings of the 25th Intersociety, 213 – 218, 1990.
- [16] M. Kotb, T. Aldoss, Flowfield around a partially-blocked Savonius rotor, *Applied Energy* 38 (2) (1991) 17–132.
- [17] N. Fujisawa, F. Gotoh, Visualization study of the flow in and around a Savonius rotor, *Experiments in Fluids* (12) (1992) 407–412.
- [18] N. Fujisawa, On the torque mechanism of Savonius rotors, *Journal of Wind Engineering and Industrial Aerodynamics* 40 (1992) 277–292.



- [19] M. S. U. K. Fernando, V. J. Modi, A numerical analysis of the unsteady flow past a Savonius wind turbine, *Journal of Wind Engineering and Industrial Aerodynamics* (32) (1989) 303–327.
- [20] V. J. Modi, M. S. U. K. Fernando, Unsteady aerodynamics and wake of the Savonius wind turbine: a numerical study, *Journal of Wind Engineering and Industrial Aerodynamics* 46-47 (1993) 811–816.
- [21] N. Fujisawa, Velocity measurements and numerical calculations of flow fields in and around Savonius rotors, *Journal of Wind Engineering and Industrial Aerodynamics* 59 (1996) 39–50.
- [22] A. Shigetomi, Y. Murai, Y. Tasaka, Y. Takeda, Interactive flow field around two Savonius turbines, *Renewable Energy* (2011) 536–545.
- [23] V. D'Alessandro, S. Montelpare, R. Ricci, A. Secchiaroli, Unsteady Aerodynamics of a Savonius wind rotor: a new computational approach for the simulation of energy performance, *Energy* 35 (8) (2010) 3349–3363.
- [24] S. Roy, U. K. Saha, Review on the numerical investigations into the design and development of Savonius wind rotors, *Renewable and Sustainable Energy Reviews* (23) (2013) 73–83.
- [25] K. Kacprzak, G. Liskiewicz, K. Sobczak, Numerical investigation of conventional and modified Savonius wind turbines, *Renewable Energy* (60) (2013) 578–585.
- [26] L. A. Danao, J. Edwards, O. Eboibi, R. Howell, A numerical investigation into the influence of unsteady wind on the performance and aerodynamics of a vertical axis wind turbine, *Applied Energy* (116) (2014) 111–124.
- [27] M. Tartuferi, V. D'Alessandro, S. Montelpare, R. Ricci, Enhancement of Savonius wind rotor aerodynamic performance: a computational study of new blade shapes and curtain systems, *Energy* 79 (2015) 371–384.
- [28] B. M. Shaughnessy, S. D. Probert, Partially-blocked savonius rotor, *Applied Energy* (43) (1992) 239–249.
- [29] I. Dobrev, F. Massouh, CFD and PIV investigation of unsteady flow through Savonius wind turbine, *Energy Procedia* (2011) 711–720.
- [30] B. Altan, M. Atilgan, The use of a curtain design to increase the performance level of a Savonius wind rotors, *Renewable Energy* 35 (4) (2010) 821–829.
- [31] S. Rolland, M. Thatcher, W. Newton, A. Williams, T. Croft, D. Gethin, M. Cross, Benchmark experiments for simulations of a vertical axis wind turbine, *Applied Energy* (111) (2013) 1183–1194.
- [32] S. Roy, U. K. Saha, Wind tunnel experiments of a newly developed two-bladed Savonius-style wind turbine, *Applied Energy* 137 (2015) 117–125.
- [33] R. Ricci, S. Montelpare, G. Borrelli, V. D'Alessandro, Experimental Analysis of a Savonius Wind Rotor for Streetlighting Systems, in: *Thermal and Environmental issue in energy systems*, Sorrento, Italy, 603–607, 2010.
- [34] M. A. Kamoji, S. B. Kedare, S. V. Prabhu, Experimental investigations on single stage modified Savonius rotor, *Applied Energy* 86 (7-8) (2009) 1064–1073.
- [35] M. Kamoji, S. Kedare, S. Prabhu, Performance tests on helical Savonius rotors, *Renewable Energy* 34 (3) (2009) 521–529.
- [36] T. Hayashi, Y. LI, Y. Hara, Wind tunnel tests on a different phase three-stage Savonius rotor, *JSME International Journal* 48 (1, series B).
- [37] J. L. Menet, A double-step Savonius rotor for local production of electricity: a design study, *Renewable Energy* 29 (11) (2004) 1843–1862.
- [38] N. Mahmoud, El-Haroun, E. Wahba, M. Nasef, An experimental study on improvement of Savonius rotor performance, *Alexandria Engineering Journal* (51) (2012) 19–25.
- [39] J. Kumburnuss, J. Chen, H. Yang, L. Lu, Investigation into the relationship of the overlap ratio and shift angle of double stage three bladed vertical axis wind turbine (VAWT), *Journal of Wind Engineering and Industrial Aerodynamics* (107-108) (2012) 57–75.
- [40] U. K. Saha, M. Rajkumar, On the performance analysis of Savonius rotor with twisted blades, *Renewable Energy* 31 (11) (2006) 1776–1788.

- 362 [41] U. K. Saha, S. Thotla, D. Maity, Optimum design configuration of Savonius rotor through wind tunnel experiments,  
363 Journal of Wind Engineering and Industrial Aerodynamics 96 (8-9) (2008) 1359–1375.
- 364 [42] A. Damak, Z. Driss, M. Abid, Experimental investigation of helical Savonius rotor with a twist of  $180^\circ$ , Renewable Energy  
365 (52) (2013) 136–142.
- 366 [43] J. V. Akwa, H. A. Vielmo, A. P. Petry, A review on the performance of Savonius wind turbines, Renewable and Sustainable  
367 Energy Reviews 16 (5) (2012) 3054 – 3064, ISSN 1364-0321.
- 368 [44] M. Nakajima, S. Iio, T. Ikeda, Performance of double-step Savonius rotor for environmentally friendly hydraulic turbine,  
369 Journal of Fluid Science and Technology 3 (3) (2008) 410–419.
- 370 [45] A. Pope, J. B. Barlow, W. H. Rae, Low-Speed Wind Tunnel Testing, John Wiley & Sons, 3rd edn., 1999.